

Antitumour activity of tin selenide nanosheets in response to ultrasound

Yafei Qin

College of Chemistry and Chemical Engineering, Central South University, Changsha, China

yafei_qin2026@163.com

Abstract. Malignant tumours are among the top ten diseases worldwide and exhibit very high morbidity and mortality. Traditional treatment methods, including radiotherapy and chemotherapy, cannot meet the urgent clinical need for cancer treatment due to poor selectivity, significant trauma, and the risk of metastasis. Sonodynamic Therapy (SDT) is an emerging tumour treatment modality. SDT based on ultrasonic-response piezoelectric nano materials demonstrates strong clinical potential due to its non-invasive nature, high efficiency, and high biosafety. Traditional acoustic sensitizers are mainly organic compounds. With the development of nanotechnology, novel acoustic sensitizers based on piezoelectric nano materials have gradually been developed. Tin selenide, a transition metal chalcogenide, is a layered (2D) semiconductor material that exhibits excellent piezoelectric properties and is expected to serve as a new type of acoustic sensitizer in tumour therapy. Tin selenide nanoparticles were synthesised using a wet chemical method with selenium powder and stannous chloride dihydrate as raw materials under alkaline conditions. Sufficient ROS were detected after ultrasonic treatment of SnSe NSs in aqueous solution under dark conditions, with the main types identified as $\cdot\text{OH}$ and $^1\text{O}_2$. The 4T1 mitoptosis test and biosafety evaluation demonstrated that SnSe NSs effectively kill tumour cells without significant toxicity to normal cells.

Keywords: piezoelectric catalysis, sonodynamic therapy, nanometer material, SnSe, ROS

1. Introduction

Malignant tumours rank among the top ten diseases globally and are characterised by exceptionally high incidence and mortality rates. According to the World Health Organisation's 2020 report [1], malignant tumours account for approximately 10 million deaths annually worldwide. Against this backdrop, improving the prevention, diagnosis, and treatment of tumours has become a critical priority.

Conventional therapeutic modalities, including radiotherapy, chemotherapy, and surgical intervention, are widely employed in clinical practice [2]. However, these approaches present significant limitations: radiotherapy and chemotherapy are often associated with substantial toxicity to normal tissues and poor selectivity of chemotherapeutic agents, while surgical procedures are highly invasive and carry a considerable risk of metastasis. These limitations have hindered the effective treatment of tumours and cancers (i.e., malignant neoplasms) [2, 3]. Consequently, the development of novel therapeutic strategies and pharmacological agents has become a key focus in biomedical research. Innovative modalities such as

Photodynamic Therapy (PDT), Sonodynamic therapy (SDT), and Photothermal Therapy (PTT) have emerged as promising alternatives for tumour treatment [4].

SDT has attracted increasing attention due to its non-invasive characteristics and strong tissue penetration capability [5]. In SDT, ultrasound acts as an external stimulus to activate sonosensitizers, which induce the generation of Reactive Oxygen Species (ROS) within or near tumour cells, leading to cellular apoptosis or necrosis [6]. Advances in nanotechnology have further enhanced SDT through the development of ultrasound-responsive piezoelectric nanomaterials [7].

During the SDT process, ultrasound energy activates the sonosensitizer, promoting its transition from the ground state to an excited state. The activated sonosensitizer reacts with molecular oxygen present in the tumour microenvironment, resulting in the production of extremely reactive ROS, including superoxide anions ($O_2^{\cdot-}$), hydrogen peroxide (H_2O_2), singlet oxygen (1O_2), and hydroxyl radicals ($\cdot OH$). The accumulation of ROS to critical levels within tumour cells induces cytotoxic effects such as decreased mitochondrial membrane potential, cytoskeletal contraction, chromatin condensation, membrane rupture, and DNA fragmentation, thereby impeding cellular proliferation. ROS primarily induce tumour cell death through protein damage, lipid oxidation, and nucleic acid disruption [4, 6, 8]. The synergistic effect of ultrasound activation and ROS generation is crucial for the modulation of tumour growth, highlighting the therapeutic potential of SDT in oncology.

The selection of appropriate sonosensitizers is crucial for SDT. Traditionally, sonosensitizers have been predominantly organic compounds, including porphyrins and their derivatives, oxime anthrone compounds, anticancer and antibacterial agents, non-steroidal anti-inflammatory drugs, and various other sonosensitizers [9]. However, these organic sonosensitizers suffer from significant limitations, such as high phototoxicity, poor accumulation, rapid metabolic degradation, and poor solubility, which restrict their clinical application [10].

Recent advancements in nanofabrication have shown that various inorganic nanomaterials—such as carbon nanotubes, mesoporous carbon nanospheres, graphene oxide, Nano-Gold (Au), Nano-Silicon Dioxide (SiO_2), Nano-Titanium Dioxide (TiO_2), Nano-Barium Titanate ($BaTiO_3$), and several magnetic nanomaterials—can respond effectively to ultrasound stimulation, facilitating the exploration and development of novel inorganic sonosensitizers through the application of nanotechnology [2]. However, inorganic sonosensitizers often exhibit inferior biocompatibility and metabolic challenges, limiting their potential for clinical use [10].

To address these challenges, researchers have developed novel sonosensitizers by incorporating organic molecules or polymers with piezoelectric nanomaterials. Piezoelectric materials possess the ability to transduce mechanical stress into electrical signals and vice versa. Common materials include $BaTiO_3$, Zinc Oxide (ZnO), and SiO_2 , and organic polymers such as Polyvinylidene Fluoride (PVDF) and nylon-11, as well as natural materials such as silk, amino acids, and collagen [7].

In recent years, tin chalcogenide compounds (SnX , where $X = S, Se, Te$) have attracted significant attention due to their applications in electronics, optics, optoelectronics, and flexible systems. These compounds are layered structures with hexagonal, monoclinic, or orthorhombic phases [11]. Tin Selenide ($SnSe$) is a representative layered (2D) semiconductor with a crystal structure similar to distorted NaCl. Atoms within its layers are interconnected by covalent bonds, forming a zigzag double-layer architecture of tin and selenium atoms. Adjacent layers are held together by weak van der Waals forces, resulting in a propensity for crystals growing along the (100) direction to adopt an orthorhombic morphology, specifically in the form of $SnSe_2$ [12].

$SnSe$ nanostructures have been widely studied due to their chemical stability, low toxicity, high biocompatibility, and large specific surface area [13]. They have shown potential in Photodynamic Therapy

(PDT) and Thermoelectric therapy (TET). For example, Tang et al. synthesised SnSe-PVP nanorods for use in photothermal and photothermal electro-dynamic therapy [14]. Furthermore, Gao et al. demonstrated that 2D SnSe nanomaterials exhibit notable catalytic activity for several dehydrogenases within cellular metabolic processes [15]. In comparison to their natural counterparts, SnSe nanosheets were observed to maintain catalytic activity exceeding 75% under a variety of reaction conditions. Additionally, SnSe holds promise for the development of antibacterial materials. Qazi et al. employed a wet chemical synthesis method to create SnSe/SnS nanocomposites, which effectively inhibited the proliferation of *Staphylococcus aureus* (a Gram-positive bacterium) and *Escherichia coli* (a Gram-negative bacterium) [16].

Despite these advances, SnSe has been insufficiently explored as a sonosensitizer for SDT. To address this research gap, the present study follows the synthesis methodology established by Yuan et al [17]. and prepares Tin Selenide Nanosheets (SnSe NSs) using a wet chemical approach under alkaline conditions, improving their solubility and stability. The study characterises and analyses their morphology, structure, particle size, and piezoelectric characteristics. Furthermore, the study examines the generation of ROS under ultrasound exposure, investigating the correlation between ROS production and the concentration of nanomaterials, as well as identifying the specific types of ROS generated. The findings demonstrate the antitumor efficacy and biocompatibility of SnSe NSs, thereby providing a foundation for their application as novel sonosensitizers in clinical sonodynamic therapy.

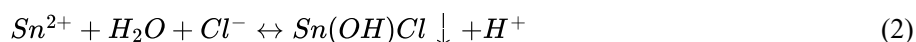
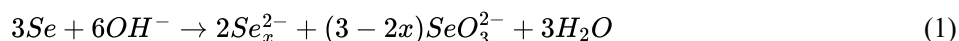
2. Results

2.1. Preparation and surface modification of snse nss

The wet chemical method was applied in this study. Selenium (Se) powder and Stannous Chloride Dihydrate ($\text{SnCl}_2 \cdot 2\text{H}_2\text{O}$) were used to synthesise Tin Selenide Nanosheets (SnSe NSs) under alkaline conditions (Figure 1). Initially, Se powder reacts with Sodium Hydroxide (NaOH) to form sodium selenite, producing solution A. Subsequently, the hydrolysis of $\text{SnCl}_2 \cdot 2\text{H}_2\text{O}$, facilitated by citric acid, causes the equilibrium of Sn^{2+} ions to shift leftward, producing solution B. After solutions A and B are fully mixed, a black flocculent precipitate begins to emerge on the liquid surface, eventually forming a black opaque suspension.

The resulting product is then subjected to centrifugation (at 11,000 rpm for 8 minutes; ThermoFisher Scientific, USA), washing, ultrasonic dispersion (Shenzhen Guanbo Technology, China), and a second centrifugation, followed by freeze-drying (Ningbo Xinzhi Biotechnology, China) to yield the final sample of SnSe NSs.

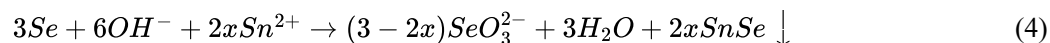
The underlying reaction mechanism is elucidated as follows, see Equation (1) and (2):



The leftward shift in the equilibrium facilitates the release of Sn^{2+} , as Equation (3):



The overall reaction can be expressed as Equation (4):



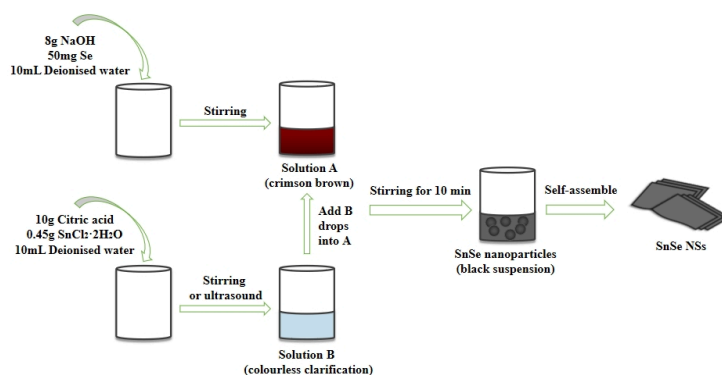


Figure 1. Schematic diagram of the synthesis of tin selenide. Upon the addition of solution B to solution A, the solution gradually changes colour from orange-red to pale yellow. A black flocculent precipitate then forms at the surface, resulting in a black, opaque suspension

The surface morphology of SnSe NSs was analysed using Scanning Electron Microscopy (SEM, JEOL, Japan) in Secondary Electron Imaging (SEI) mode, with an acceleration voltage set at 10.0 kV and a working distance of 7.3 mm (Figure 2). The SEM images show that SnSe NSs predominantly exhibit a stacked, sheet-like structure, with individual sheets presenting a relatively uniform rectangular shape and an approximate width of 200 nm.

Previous studies indicate that the concentration of the alkaline solution significantly affects the morphology and structural characteristics of SnSe. At a NaOH concentration of 5 M, nanoscale particles are predominantly formed, whereas a concentration of 10 M favours the formation of tin SnSe nanosheets [17]. Based on the SEM observations, it is therefore likely that a sodium hydroxide concentration slightly below 10 M contributed to the formation of poorly defined strip-like and fragmented structures.

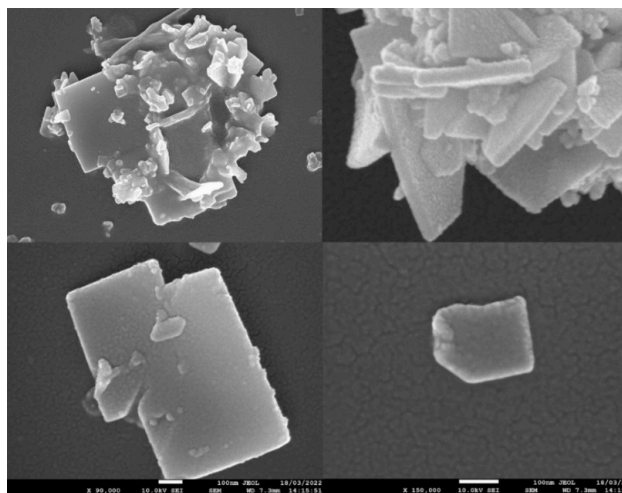


Figure 2. SEM images of SnSe NSs showing a distinct rectangular sheet-like structure

X-Ray Diffraction (XRD) analysis was conducted using an X-ray diffractometer (RIGAKU, Japan) over a 2θ range of 10° to 70° . Comparison with the standard XRD card JCPDS No. 48-1224 shows that the diffraction peaks corresponding to (101), (201), (210), (011), (111), (400), (311), (102), (411), (020), (302),

(511), (131), (811), and (522) exhibited strong alignment with the reference pattern (Figure 3). These results confirm the orthorhombic phase of SnSe, confirming the structural integrity of the synthesised nanostructures.

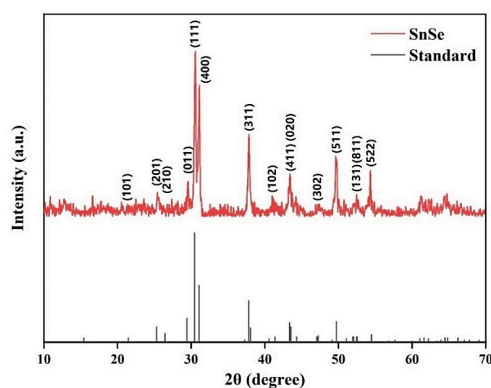


Figure 3. X-ray diffraction spectrum of SnSe NSs, showing a strong correlation with the reference pattern, indicating high crystallinity and phase purity

To improve stability and water solubility, SnSe NSs were surface-modified with Hyaluronic acid (HA), yielding HA-SnSe NSs. The particle size and zeta potential before and after modification were analysed using a Size-Zeta particle size and potential analyser (Malvern Instruments, UK) under controlled conditions (temperature: 25.0 °C, equilibrium time: 0, sample cell: DTS060C). Before modification, the average particle size of SnSe NSs was approximately 900 nm. After HA modification, the size decreased to approximately 80 nm (Figure 4). This reduction is attributed to the aggregation tendency of unmodified SnSe NSs, while the introduction of HA significantly improved the dispersion of the nanomaterials in aqueous solutions, resulting in nanoscale particles.

Furthermore, the zeta potential of the unmodified SnSe NSs was observed to be positive; after modification, this value shifted to negative, accompanied by a substantial increase in its absolute value. This indicates that the initially positively charged SnSe NSs acquired a negative charge upon modification (Figure 5). Given that the surface of tumour cells generally exhibits a positive charge, the modified SnSe NSs could potentially be attracted to the vicinity of tumour cells through electrostatic interactions, thereby demonstrating significant promise for anti-tumour applications. The observed increase in the zeta potential value subsequent to modification further signifies a reduction in particle size and an enhancement of the stability of the nanosystem. Collectively, these findings indicate that the surface modification of SnSe NSs successfully achieved the intended outcomes.

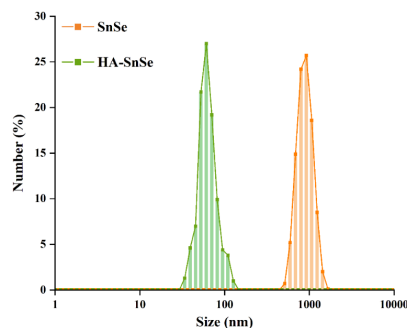


Figure 4. Particle size distribution of SnSe NSs before and after HA modification, showing significant size reduction

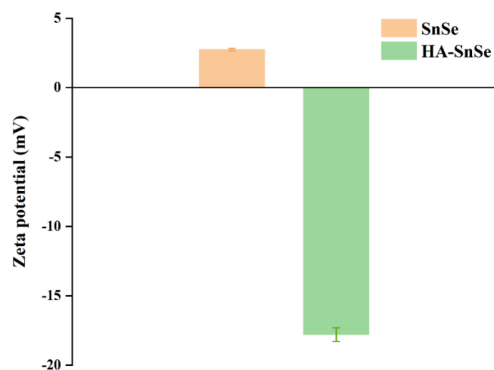


Figure 5. Zeta potential of SnSe NSs before and after HA modification, indicating a shift from positive to negative surface charge and improved stability

2.2. In vitro ROS generation effect of SnSe NSs

2.2.1. The effect of varying concentrations of SnSe NSs on ROS generation

In aqueous solutions, SnSe NSs exhibit catalytic properties that promote the generation of ROS in surrounding materials when triggered by ultrasound. These ROS subsequently react with DCFH (initially non-fluorescent, generated by hydrolysis between 2',7'-Dichlorodihydrofluorescein Diacetate (DCFH-DA) with NaOH) to produce DCF. This reaction results in the emission of fluorescence peaks at specific wavelengths, thereby providing a measurable indication of oxidative activity. The reaction pathway is as follows, see Equation (5):



DCFH (100 $\mu\text{g/mL}$, pH = 7) was used as a fluorescent probe and mixed with SnSe NSs at a concentration of 400 $\mu\text{g/mL}$ in a 1:1 (v/v) ratio. A control mixture comprised of DCFH and deionised water in a 1:1 (v/v) ratio was also prepared. Four experimental groups were established: (1) control group (DCFH + water); (2) Ultrasound (US) group (DCFH + water, US treatment); (3) SnSe NSs group (DCFH + SnSe NSs); and (4) SnSe NSs + US group (DCFH + SnSe NSs, US treatment). To prevent light exposure, all samples were

wrapped in aluminium foil. Ultrasound treatment was applied to groups (2) and (4) using an ultrasonic therapy device (Shenzhen Weirde Medical, China), while groups (1) and (3) remained untreated.

Ultrasound was applied at an acoustic intensity of 1.00 W/cm² for 5 minutes, followed by a 5-minute interval, repeated for three cycles. After treatment, supernatants from groups (3) and (4) were collected by centrifugation. Fluorescence emission spectra of all groups were then analysed using an F-4600 fluorescence spectrophotometer (Hitachi, Japan) with an excitation wavelength set at 480 nm and an emission range of 500-600 nm.

All groups exhibited a fluorescence peak at approximately 525 nm. However, the control and US groups showed minimal fluorescence at this wavelength. In contrast, both the SnSe NSs group and the SnSe NSs + US group exhibited strong fluorescence at 525 nm, with the latter showing significantly higher intensity. These findings suggest that SnSe NSs are capable of generating substantial quantities of ROS when subjected to ultrasound treatment. It was also observed that the SnSe NSs group demonstrated considerable fluorescence, likely due to the ability of SnSe NSs in an aqueous environment to catalyse ROS generation. However, the fluorescence intensity was considerably lower than that in the SnSe NSs + US group, indicating that the ROS within the aqueous system were predominantly produced via the catalytic action of SnSe NSs induced by ultrasound treatment (Figure 6).

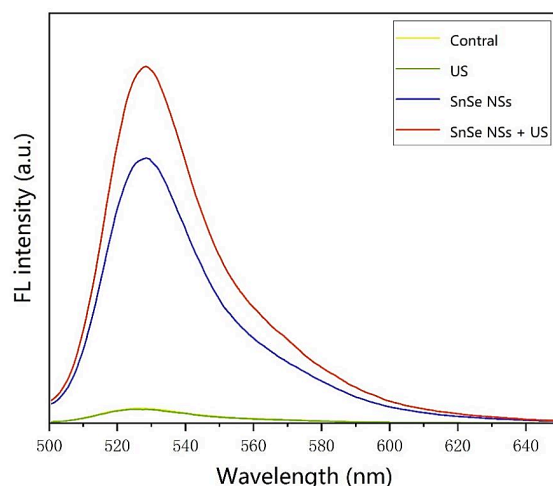


Figure 6. Fluorescence emission spectrum of the DCFH-DA reagent utilised to assess the production of ROS by SnSe NSs. The SnSe NSs + US group exhibited the highest fluorescence intensity, followed by the SnSe NSs group. In contrast, both the control group and the US group demonstrated negligible fluorescence emission peaks around 528 nm

To further investigate the effect of SnSe NS concentration on ROS generation and determine the optimal concentration, a series of experiments was conducted. A DCFH solution at a concentration of 100 µg/mL was mixed in a 1:1 (v/v) ratio with SnSe NSs at varying concentrations of 50, 100, 200, 300, 400, 500, and 600 µg/mL. As a control, the DCFH reagent was combined with deionised water in a 1:1 (v/v) ratio. Following the same ultrasound treatment, fluorescence emission spectra were measured at an excitation wavelength of 525 nm.

The results revealed a non-linear relationship between SnSe NS concentration and fluorescence intensity, initially increasing before subsequently decreasing (Figure 7). The maximum fluorescence intensity was

observed at concentrations of 150 $\mu\text{g/mL}$ and 200 $\mu\text{g/mL}$, with the intensity at 200 $\mu\text{g/mL}$ being marginally higher than that at 150 $\mu\text{g/mL}$. In contrast, concentrations at or below 50 $\mu\text{g/mL}$, as well as in the control and US group, yielded relatively low fluorescence intensities, which were nearly negligible. When the concentration of SnSe NSs was below 200 $\mu\text{g/mL}$, the increase in concentration correlated with an enhancement in ROS production due to ultrasound stimulation, resulting in a corresponding increase in fluorescence intensity. However, at concentrations exceeding 200 $\mu\text{g/mL}$, a decline in fluorescence intensity was observed. This phenomenon may be attributed to the aggregation of SnSe NSs in solution at higher concentrations, which potentially obstructs their catalytic efficacy in facilitating ROS generation under ultrasonic conditions. In conclusion, the optimal concentration of SnSe NSs for enhancing ROS generation through piezoelectric catalysis is identified as 200 $\mu\text{g/mL}$.

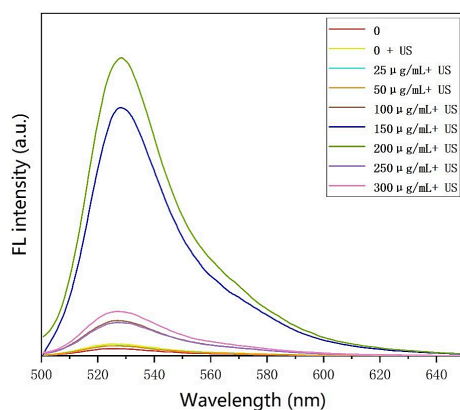


Figure 7. Fluorescence emission spectra of ROS generated by the ultrasonic activation of SnSe NSs at varying concentrations

2.2.2. Analysis of ROS species generated by piezoelectric catalysis of SnSe NSs

ROS encompass a variety of chemically reactive oxygen-containing molecules, including superoxide anions ($\text{O}_2^{\cdot-}$), Hydrogen Peroxide (H_2O_2), Hydroxyl Radicals ($\cdot\text{OH}$), Ozone (O_3), and Singlet Oxygen ($^1\text{O}_2$). To elucidate the specific types of ROS generated by SnSe NSs and to facilitate the investigation of their underlying piezoelectric catalytic mechanisms, various detection methods were employed for measurement and analysis.

In examining the potential ROS produced by SnSe NSs, Terephthalic acid (1,4-Dicarboxybenzene, TA) was selected to assess the generation of $\cdot\text{OH}$ and to quantify the extent of its production. Additionally, Singlet Oxygen Sensor Green (SOSG), a singlet oxygen fluorescent probe, was utilized to investigate the generation and efficiency of $^1\text{O}_2$. Lastly, an Amplex Red fluorescent probe was employed to confirm the production of H_2O_2 and evaluate its generation level.

2.2.2.1. Verification and analysis of $\cdot\text{OH}$ generation from SnSe NSs

Terephthalic Acid (TA) is known to react with $\cdot\text{OH}$ to form 2-Hydroxyterephthalic Acid (HTA), a compound that exhibits strong fluorescence properties. Due to this characteristic, TA is frequently employed as a specific fluorescent probe for the detection of $\cdot\text{OH}$. The detailed reaction pathway is as Equation (6):



Using the same ultrasonic cycling parameters outlined in Section 2.2.1, four experimental groups were established: (1) Control group (TA + water); (2) US group (TA + water, US treatment); (3) SnSe NSs group (TA + SnSe NSs); (4) SnSe NSs + US group (TA + SnSe NSs, US treatment). All samples were wrapped in aluminium foil to prevent exposure to light. The fluorescence emission spectrum of $\cdot\text{OH}$ generated by SnSe NSs under ultrasonic stimulation was analysed (excitation wavelength of 315 nm and emission range of 350-500 nm).

A pronounced fluorescence peak was observed at 425 nm in the experimental groups, with the SnSe NSs + US group exhibiting the highest fluorescence intensity, while both the control group and the SnSe NSs group displayed negligible fluorescence. Furthermore, the fluorescence intensity in the US group was significantly higher than that of the control and SnSe NSs group, although it remained lower than that of the SnSe NSs + US group (Figure 8). This observed phenomenon may be attributed to the catalysis of free radical generation from water by the ultrasonic treatment. These results suggest that the primary source of $\cdot\text{OH}$ in the aqueous system is the piezoelectric catalytic activity of SnSe NSs induced by ultrasound.

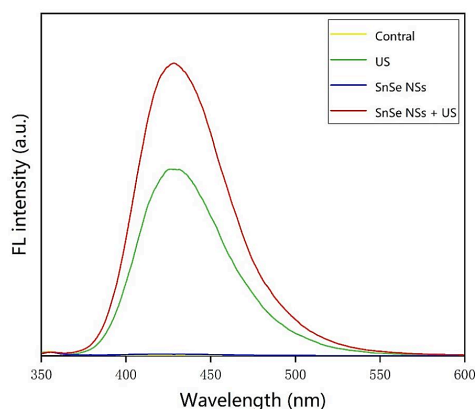


Figure 8. Fluorescence emission spectrum of $\cdot\text{OH}$ generated through the piezo-catalytic activity of SnSe NSs in the presence of TA reagent. The results indicate that the fluorescence intensity of the SnSe NSs + US group is significantly higher compared to the control group, while both the control and SnSe NSs groups exhibit minimal fluorescence intensity. The final concentration of SnSe NSs was maintained at 200 $\mu\text{g}/\text{mL}$, and the final concentration of the TA reagent was approximately 0.3 mM in this experiment

2.2.2.2. Verification and analysis of $^1\text{O}_2$ generation from SnSe NSs

The singlet oxygen fluorescence probe, Singlet Oxygen Sensor Green (SOSG), serves as a highly selective reagent for the detection of $^1\text{O}_2$, exhibiting minimal responsiveness to $\cdot\text{OH}$ and $\text{O}_2^{\cdot-}$. This selectivity enables the specific quantification of $^1\text{O}_2$. In aqueous solutions, the intensity of the resulting green fluorescence signal is directly correlated with the concentration of $^1\text{O}_2$. Thus, by analysing the fluorescence emission spectra of the SnSe NSs solution containing SOSG, the efficacy of SnSe NSs in generating $^1\text{O}_2$ can be evaluated.

Four experimental groups were established using the same ultrasonic cycling setup as described in section 2.2.1: (1) control group (HEPES buffer + SOSG); (2) US group (HEPES buffer + SOSG, US treatment); (3) SnSe NSs group (HEPES buffer + SOSG + SnSe NSs); (4) SnSe NSs + US group (HEPES buffer + SOSG + SnSe NSs, US treatment), with all samples wrapped in aluminium foil to prevent exposure to light. The fluorescence emission spectrum associated with $^1\text{O}_2$ was measured (excitation wavelength of 488 nm; emission range of 500-650 nm) (Figure 9). A significant fluorescence peak was observed at 535 nm in the experimental

groups, which is close to the maximum emission wavelength of SOSG at 525 nm. The SnSe NSs + US group exhibited the highest fluorescence intensity, followed by the US group, which may be attributed to the inherent catalytic effect of ultrasound on water, leading to the generation of a small amount of $^1\text{O}_2$. Although the control group and the SnSe NSs group demonstrated a degree of fluorescence, their intensities were considerably lower than that of the SnSe NSs + US group. These findings suggest that the primary source of $^1\text{O}_2$ in the aqueous medium is from the piezoelectric catalysis of SnSe NSs induced by ultrasound.

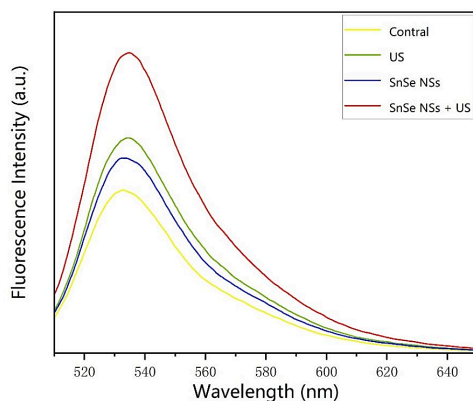
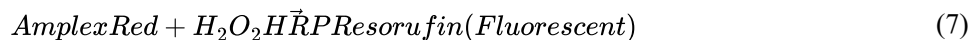


Figure 9. Fluorescence emission spectrum of $^1\text{O}_2$ generated through ultrasonic-triggered piezo-catalysis of SnSe NSs detected using the SOSG. The SnSe NSs + US group exhibits the highest fluorescence intensity, followed by the US group, while the control and SnSe NSs groups display comparatively lower fluorescence intensities. The final concentration of SnSe NSs utilised in this experiment was 200 $\mu\text{g}/\text{mL}$, and the final concentration of SOSG was maintained at 2.5 μM . The HEPES buffer concentration was set at 10 mM with a pH of 6.8

2.2.2.3. Verification and analysis of H_2O_2 generation from SnSe NSs

10-acetyl-3,7-dihydroxyphenoxazine, commonly referred to as Amplex Red, serves as a highly sensitive fluorescent probe for H_2O_2 and various peroxidases. In the presence of peroxidases such as Horseradish Peroxidase (HRP) and Myeloperoxidase (MPO), Amplex Red reacts with H_2O_2 in a 1:1 ratio to produce a strongly fluorescent product known as Resorufin. The underlying reaction mechanism can be elucidated as follows, see Equation (7):



SnSe NSs were dispersed in a 0.85% sodium chloride solution, and the resulting filtrate was obtained using a polyvinylidene fluoride membrane. Four experimental groups were established utilising the same ultrasonic cycling setup described in Section 2.2.1: (1) control group (Amplex Red + HRP phosphate buffer); (2) US group (Amplex Red + HRP phosphate buffer, US treatment); (3) SnSe NSs group (Amplex Red + HRP phosphate buffer + SnSe NSs); (4) SnSe NSs + US group (Amplex Red + HRP phosphate buffer + SnSe NSs, US treatment), with all samples wrapped in aluminium foil to avoid light exposure.

The fluorescence emission spectrum of H_2O_2 generated under ultrasonic stimulation was measured (excitation wavelength: 530 nm; emission range: 560-750 nm). A pronounced fluorescence intensity was observed at 600 nm in the experimental groups, with the SnSe NSs + US group exhibiting the highest intensity, followed by the SnSe NSs group with slightly lower intensity (Figure 10). In contrast, the control

and US groups showed negligible fluorescence. It is speculated that the SnSe NSs present in the aqueous solution possess an inherent ability to catalyse the production of H_2O_2 from surrounding substances, and that ultrasonic treatment significantly enhances this catalytic activity. Therefore, SnSe NSs, when subjected to ultrasonic stimulation, exhibit superoxide dismutase-like activity.

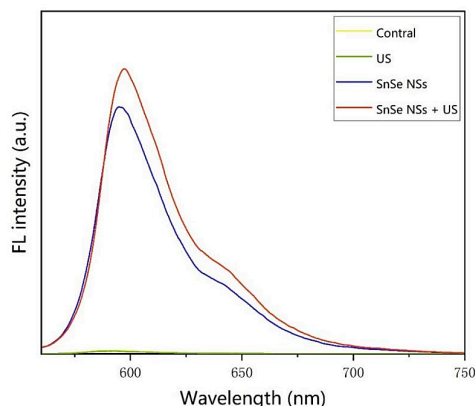


Figure 10. Fluorescence emission spectrum of H_2O_2 generated through ultrasound-triggered piezo-catalysis of SnSe NSs detected using Amplex Red. The fluorescence intensity observed in the SnSe NSs + US group is the highest among all tested conditions. In comparison, the fluorescence intensity of the SnSe NSs group is slightly lower than that of the SnSe NSs + US group. In contrast, both the control group and the US group exhibit negligible fluorescence. The final concentration of SnSe NSs utilised in this experiment was 200 $\mu\text{g/mL}$, while the final concentration of Amplex Red was approximately 0.013 g/L

2.3. Antitumour effects and biosafety evaluation of SnSe NSs

2.3.1. Antitumour effects of SnSe NSs

Apoptosis plays a crucial role in tumour monitoring. In healthy cells, the mitochondrial transmembrane potential is typically high, whereas in damaged or apoptotic cells, this indicator is reduced. The reduction of mitochondrial membrane potential usually serves as an early biomarker for apoptosis and can be utilised to assess the status of tumour cells. The JC-1 probe can traverse the mitochondrial membrane and accumulate in the matrix to form aggregates that emit strong red fluorescence. In apoptotic cells, however, the mitochondrial transmembrane potential decreases due to depolarisation, leading to the release of the JC-1 probe from the mitochondria at lower concentrations, resulting in the probe existing as monomers that emit green fluorescence, in contrast to the aggregates. Consequently, qualitative detection of changes in mitochondrial membrane potential can be achieved through variations in fluorescence colour, while the relative proportions of red and green fluorescence can be used to quantitatively assess the extent of mitochondrial depolarisation.

In this study, mouse breast cancer cells (4T1 cells) were used as the model cell line. Four experimental groups were established: (1) Control group (culture medium); (2) US group (culture medium, US treatment); (3) SnSe NSs group (culture medium + SnSe NSs); (4) SnSe NSs + US group (culture medium + SnSe NSs, US treatment). 4T1 cells were seeded in 96-well plates and incubated with the above four solutions for 24 hours. Groups (2) and (4) underwent the same ultrasound cycling procedure described in Section 2.2.1, after which JC-1 staining solution was added, and the cells were incubated at 37°C for 20 minutes. Mitochondrial staining was examined using a fluorescence inverted microscope (OLYMPUS, Japan).

Figure 11 presents fluorescence images reflecting mitochondrial membrane potential for each group: (a) and (e), (b) and (f), (c) and (g), and (d) and (h) correspond to the control group, US group, SnSe NSs group, and SnSe NSs + US group, respectively. The results indicate that red fluorescence predominated in the control, US, and SnSe NSs groups compared to the green fluorescence. In contrast, the SnSe NSs + US group exhibited a predominance of green fluorescence, with pronounced green fluorescence observed in extensive aggregated areas, which suggests the 4T1 cells in the control, US, and SnSe NSs groups were growing effectively, while the cells in the SnSe NSs + US group displayed substantial cell death. These findings demonstrate that neither ultrasound nor SnSe NSs alone significantly affects the growth of 4T1 cells, whereas their combined application exerts a potent cytotoxic effect on tumour cells. This highlights the considerable potential of synthesised SnSe NSs for ultrasound-responsive anti-tumour therapies.

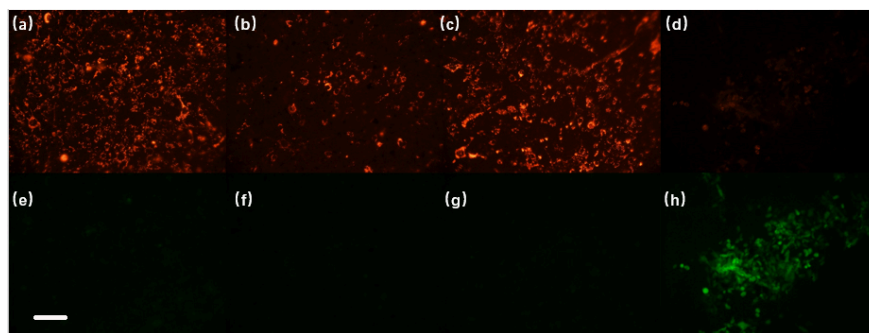


Figure 11. Assessment of mitochondrial membrane potential in 4T1 cells using the JC-1 probe (scale bar = 50 μm). (a) and (e), (b) and (f), (c) and (g), and (d) and (h) depict fluorescent images across the control group, US group, SnSe NSs group, and SnSe NSs + US group, respectively. An excitation wavelength of 490 nm and emission wavelength of 530 nm were used to detect green fluorescence (apoptotic cells), while an excitation wavelength of 525 nm and emission wavelength of 590 nm were used to detect red fluorescence (viable cells)

2.3.2. Biosafety evaluation of SnSe NSs

Cell toxicity assessments were conducted to evaluate the biocompatibility of SnSe NSs. Human Umbilical Vein Endothelial Cells (HUVECs) were selected as the model cell line. Cell viability after incubation with varying concentrations of SnSe NSs was determined using a Cell Counting Kit-8 (CCK-8) assay. Absorbance measurements of SnSe NSs at concentrations of 25, 50, 100, 150, and 200 $\mu\text{g/mL}$ were obtained at a wavelength of 450 nm using an enzyme-linked immunosorbent assay (ELISA). Cell viability was calculated according to the following formula, as Equation (8):

$$\text{Cellviability} = \frac{A_s - A_b}{A_c - A_b} \times 100\% \quad (8)$$

where A_s represents the absorbance of the experimental group (HUVECs, culture medium, CCK-8, and SnSe NSs), A_c represents the control group (HUVECs, culture medium, and CCK-8), and A_b represents the blank group (culture medium, CCK-8, and SnSe NSs).

The results indicate that, within the tested concentration range (0-200 $\mu\text{g/mL}$), cell viability remains above 70% across all concentrations (Figure 12). Notably, the lowest viability (approximately 73%) occurs at 100 $\mu\text{g/mL}$. Importantly, at 200 $\mu\text{g/mL}$ —the concentration that produces the highest level of ROS—cell viability remains relatively high at 89%. These findings suggest that the concentrations of SnSe NSs utilised in this study align with established criteria for biological safety.

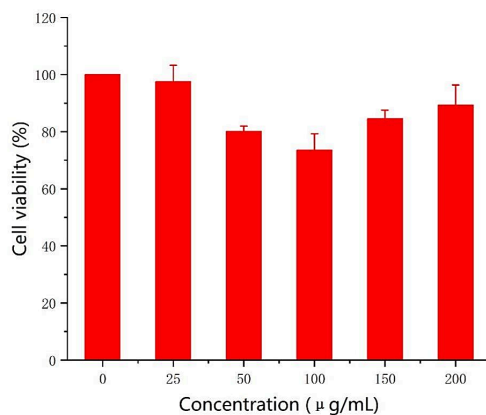


Figure 12. Cell viability of HUVECs following incubation with varying concentrations of SnSe NSs, as assessed by the CCK-8 assay. Cell viability remains approximately 89% at the optimal concentration

3. Conclusion

The remarkable piezoelectric properties of Tin Selenide (SnSe) demonstrate significant potential for ultrasonic-triggered ROS generation in piezo-catalytic tumour therapy. In this study, two-dimensional, flake-like SnSe nanomaterials were synthesised via a wet-chemistry approach, resulting in a rectangular stacked structure with an average single-layer width of approximately 500 nm. The XRD pattern of the SnSe NSs was compared with standard reference cards and exhibited strong correlation, with all observed diffraction peaks indicating the orthorhombic phase of SnSe. Following modification with hyaluronic acid, the average particle size decreased to approximately 80 nm, while the Zeta potential transitioned from positive to negative with an increased absolute value, significantly enhancing solubility and stability in aqueous environments.

The SnSe NSs in an aqueous solution exhibited a piezoelectric catalytic effect upon ultrasonic treatment, inducing surrounding water molecules to generate ROS. The amount of ROS produced is concentration-dependent, increasing initially and then decreasing, with a peak at 200 µg/mL. Using DCFH, TA, SOSG, and Amplex Red reagents, various types of ROS—including total ROS, $O_2^{\cdot-}$, H_2O_2 , $\cdot OH$, and 1O_2 —were detected. The results suggest that SnSe NSs are capable of generating substantial amounts of ROS, with $\cdot OH$ and 1O_2 being the predominant species.

Furthermore, cell viability assays and biosafety assessments confirm that SnSe NSs can effectively induce apoptosis in tumour cells while exhibiting minimal cytotoxicity towards healthy human cells, indicating strong anti-tumour efficacy with acceptable biosafety. Although SnSe nanomaterials have been explored in various biomedical applications, their use in sonodynamic therapy remains largely unexplored. Given their favourable biocompatibility and functional properties, SnSe nanomaterials show considerable promise as novel sonosensitisers for future clinical applications in cancer treatment.

References

- [1] World Health Organization. (2020). *World health statistics 2020: Monitoring health for the SDGs*. World Health Organization. <https://www.who.int/publications/i/item/9789240005105>
- [2] Wen, P., & Shi, F. (2021). Research progress of nanomaterials in tumor therapy. *Anti-Tumor Pharm.*, 11(2), 153–157+164.

- [3] Meng, L. (2009). *Theoretical study and acoustic field design simulation of ultrasound-controlled micro-nano drug particles*. Northeastern University.
- [4] Chen, L., Xu, P., Wang, S., & Chen, A. (2021). Research progress of tumor sonodynamic therapy based on nanomaterials. *Chin. Sci. Bull.*, 66(9), 1057–1066.
- [5] Zhang, Z., Yang, D., Zhang, X., Fu, Q., Yue, Y., Pu, X., Li, M., Gu, X., & Xu, Y. (2021). Research progress of sonodynamic therapy. *J. Clin. Ultrasound Med.*, 23(8).
- [6] Yang, H., & Cheng, W. (2021). Mechanisms and advances of sonodynamic therapy for tumor treatment. *J. Med. Imaging*, 31(7), 1247–1249.
- [7] Xu, Q., Gao, X., Zhao, S., Liu, Y.-N., Zhang, D., Zhou, K., Khanbareh, H., Chen, W., Zhang, Y., & Bowen, C. (2021). Construction of bio-piezoelectric platforms: From structures and synthesis to applications. *Adv. Mater.*, 33(27), 2008452.
- [8] Cafarelli, A., Marino, A., Vannozzi, L., Puigmartí-Luis, J., Pané, S., Ciofani, G., & Ricotti, L. (2021). Piezoelectric nanomaterials activated by ultrasound: The pathway from discovery to future clinical adoption. *ACS Nano*, 15(7), 11066–11086.
- [9] Zhao, W., Li, C., Xu, Z., Xu, S., & Zhang, M. (2021). Research progress of sonodynamic therapy for cancer. *Chin. J. Laser Med. Surg.*, 30(5), 275–282.
- [10] Cheng, Z., Liang, S., & Lin, J. (2021). *Developing novel sonosensitizers for sonodynamic therapy of tumors*. In Proceedings of the China Rare Earth Society Annual Academic Conference (Chengdu).
- [11] Shi, W., Gao, M., Wei, J., Gao, J., Fan, C., Ashalley, E., Li, H., & Wang, Z. (2018). Tin selenide (SnSe): Growth, properties, and applications. *Adv. Sci.*, 5(4), 1700602.
- [12] Li, L., Chen, Z., Hu, Y., Wang, X., Zhang, T., Chen, W., & Wang, Q. (2013). Single-layer single-crystalline SnSe nanosheets. *J. Am. Chem. Soc.*, 135(4), 1213–1216.
- [13] Zhu, K., Tang, Y., Zhong, X., Xiong, L., Zhang, Y., Tan, C., Song, H., & Wang, J. (2020). Improved response/recovery time and sensitivity of SnSe nanosheet humidity sensor by LiCl incorporation. *Adv. Electron. Mater.*, 6(5), 1901330.
- [14] Tang, Z., Zhao, P., Ni, D., Liu, Y., Zhang, M., Wang, H., Zhang, H., Gao, H., Yao, Z., & Bu, W. (2018). Pyroelectric nanoplatform for NIR-II-triggered photothermal therapy with simultaneous pyroelectric dynamic therapy. *Mater. Horiz.*, 5(5), 946–952.
- [15] Gao, M., Wang, Z., Zheng, H., Wang, L., Xu, S., Liu, X., Li, W., Pan, Y., Wang, W., Cai, X., Wu, R., Gao, X., & Li, R. (2020). Two-dimensional tin selenide (SnSe) nanosheets capable of mimicking key dehydrogenases in cellular metabolism. *Angew. Chem. Int. Ed.*, 59(9), 3618–3623.
- [16] Qazi, A., Nazir, M., Shahid, M., Butt, S., & Basit, M. A. (2021). Facile development of hybrid bulk-nanostructured SnSe/SnS for antibacterial activity with negligible cytotoxicity. *J. Clust. Sci.*, 32(3), 665–672.
- [17] Yuan, S., Zhu, Y.-H., Li, W., Wang, S., Xu, D., Li, L., Zhang, Y., & Zhang, X.-B. (2017). Surfactant-free aqueous synthesis of pure single-crystalline SnSe nanosheet clusters as anode for high energy- and power-density sodium-ion batteries. *Adv. Mater.*, 29(4), 1602469.